Earth's Future

Supporting Information for

Contrasting drought propagation into the terrestrial water cycle between dry and wet regions

Wantong Li[1*], Markus Reichstein[1,2], Sungmin O[3], Carla May[1], Georgia Destouni[4], Mirco Migliavacca[5], Basil Kraft[1], Ulrich Weber[1] and René Orth[1]

[1]Department of Biogeochemical Integration, Max Planck Institute for Biogeochemistry, Germany.

[2]Integrative Center for Biodiversity Research (iDIV), Leipzig, Germany.

[3]Department of Climate & Energy System Engineering, Ewha Womans University, Seoul, Korea.

[4]Department of Physical Geography, Bolin Center for Climate Research, Stockholm University, Stockholm, Sweden.

[5]European Commission, Joint Research Centre (JRC), Ispra, Italy.

*Corresponding author: Wantong Li (wantong@bgc-jena.mpg.de)

Contents of this file

Table S1: Input variables to produce machine-learning-based soil moisture, evaporation, and runoff products.

Machine-learning products	Input variables	Target variables
SoMo.ml (O & Orth 2021)	ERA5 soil moisture is used to adjust the mean and standard deviation of in-situ soil moisture ERA5 meteorological forcing Static data: climate data from ERA5, topograph data from ETOPO1, vegetation and soil types from GLDAS	ISMN in-situ soil moisture measurements from 0 to 50 cm
FLUXCOM RS (Jung et al., 2019)	Eddy covariance net radiation, and sensible heat MODIS data related to radiation, land surface temperature, vegetation indices, and plant functional types	FLUXNET Eddy covariance latent energy
G-RUN (Ghiggi et al., 2021)	21 global gridded precipitation and 2-m air temperature from e.g., CRU TS v4.04, GSWP3, MERRA, ERA5, and PGFv2 (see Fig. 1 in Ghiggi et al., 2021)	The Global Streamflow Indices and Metadata Archive River discharge data

Table S2: Depths of total soil moisture in land surface models.

Land surface models	Depths of total soil moisture (unit: m)
ISAM	3.25
LPX-Bern	Two buckets; depths are not denoted
CLM5.0	8.6
JSBACH	0.91
JULES	3
ORCHIDEE-CNP	2
LPJ-GUESS	1.5
VISIT	Depending on rooting depths; maximum 2 m
CABLE-POP	2.872

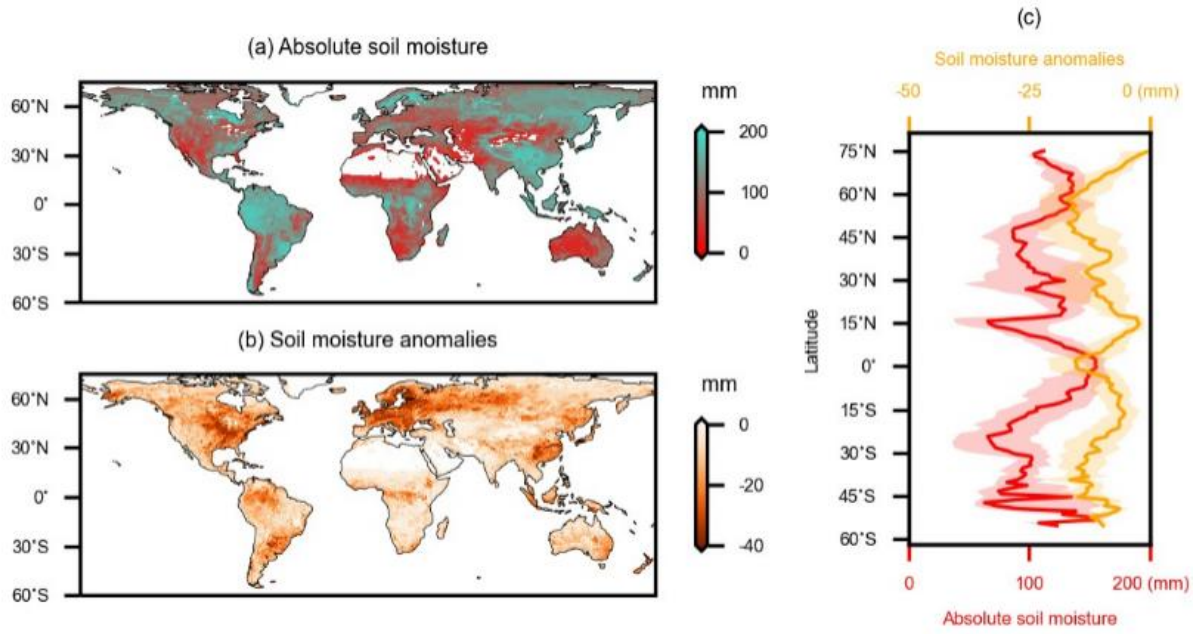

Figure S1: Mapping (a) absolute soil moisture and (b) soil moisture anomalies at drought peaks. (c) Latitudinal patterns of displayed absolute soil moisture and soil moisture anomalies. In (c), the solid line and shaded areas show the median and interquartile ranges of absolute soil moisture and soil moisture anomalies across latitudes, respectively.

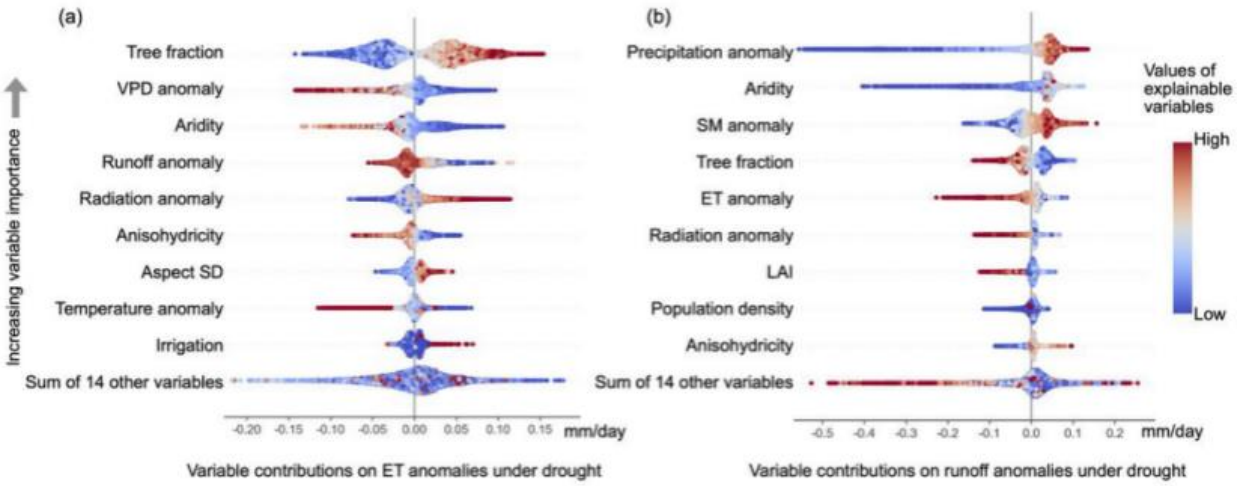

Figure S2: Variables regulating (a) ET and (b) runoff drought responses. Relative importance is shown by the order of explanatory variables in the y-axis. Positive (negative) contributions of these variables on ET or runoff anomalies at drought peaks are shown in the x-axis in each row. Red (blue) colors indicate larger (smaller) values of explanatory variables. Colors combined with signs of the x-axis values indicate positive or negative relationships between explanatory variables and water fluxes drought responses, e.g. high tree fraction contributes positively to ET anomalies (red data points contribute to ET in the value range mostly between 0-0.15 mm/day) in the first row. SD denotes the standard deviation. All plotting variables plus 14 not shown variables in each subplot are summarized in Table 1.

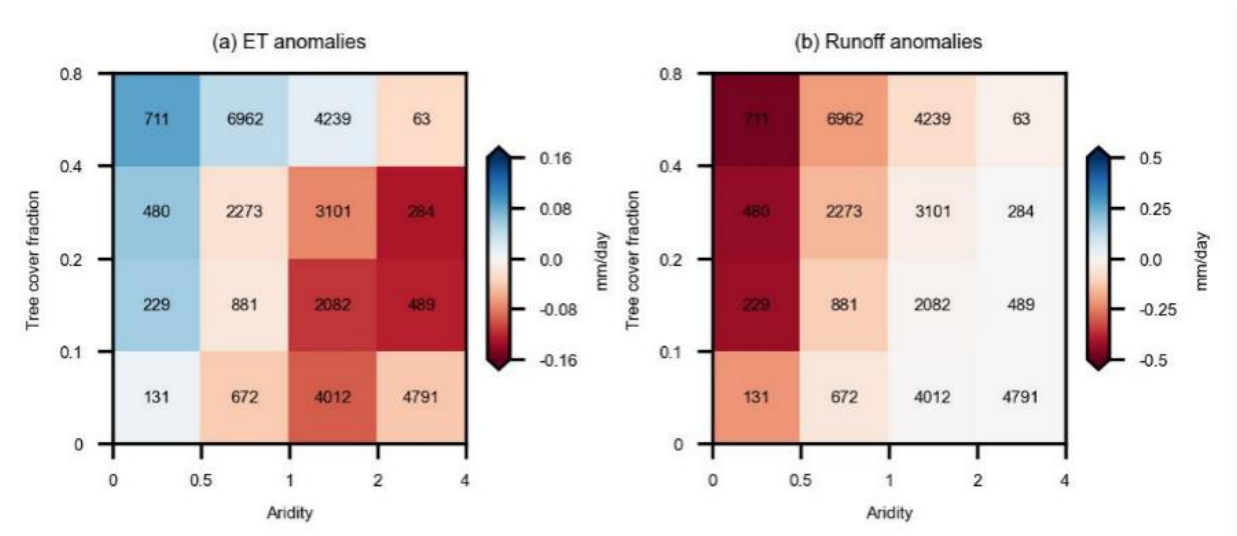

Figure S3: Similar to Figure 3, but regions with aridity > 4 are excluded in this figure due to less in-situ soil moisture observations.

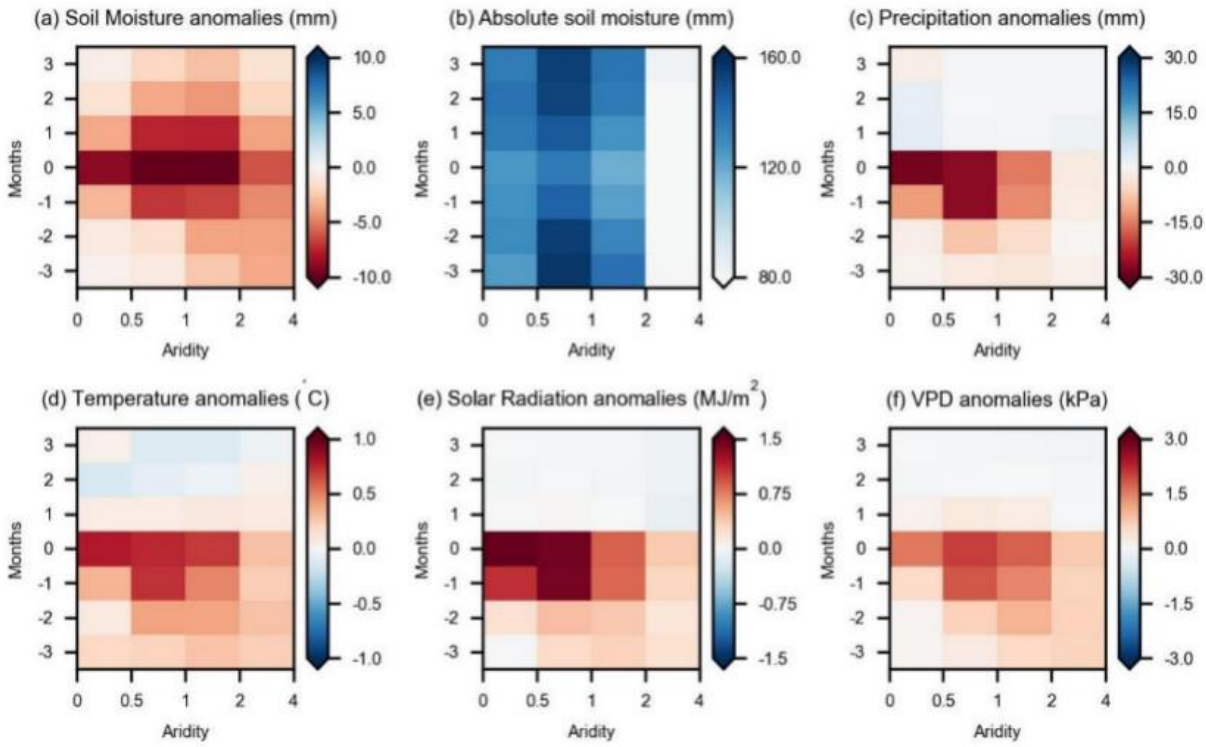

Figure S4: Hydro-climate-condition changes during the course of drought from ERA5-land reanalysis grouped by aridity expressed as medians across grid cells. Month 0 denotes the drought peak months; negative months (-3, -2, -1) denote drought development periods and positive months (1, 2, 3) denote the drought recovery periods.

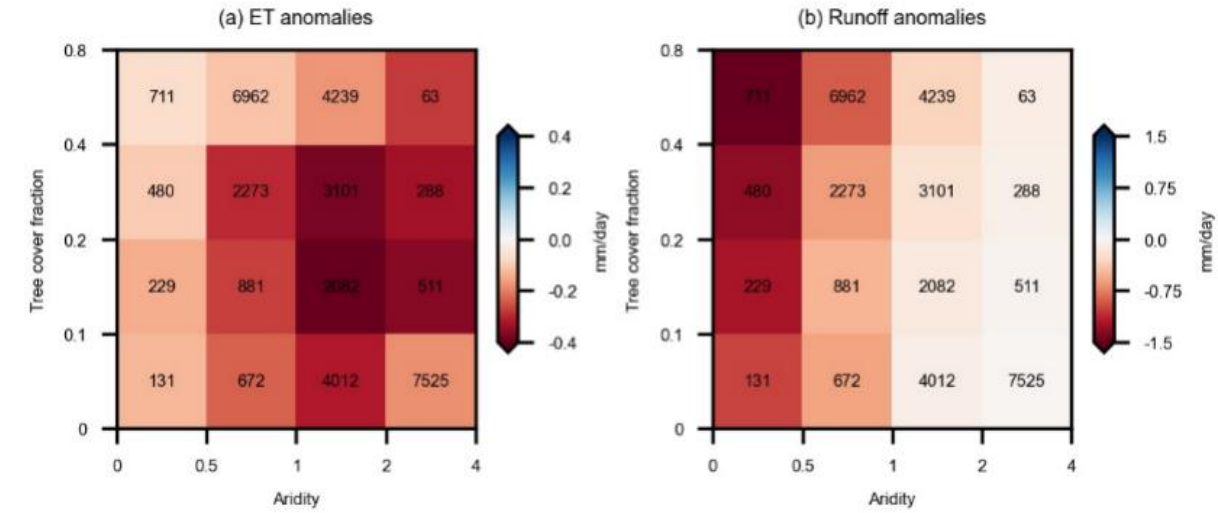

Figure S5: (a) ET and (b) runoff anomalies at drought peaks expressed as the 25th percentile of value ranges across aridity and tree cover regimes. The number in each box indicates the amount of global grid cells in each regime. Aridity is computed as the ratio between long-term net radiation and precipitation, higher values indicate drier conditions. A few grid cells showing tree cover fraction over 0.8 are moved to the 0.4-0.8 group for simplicity.

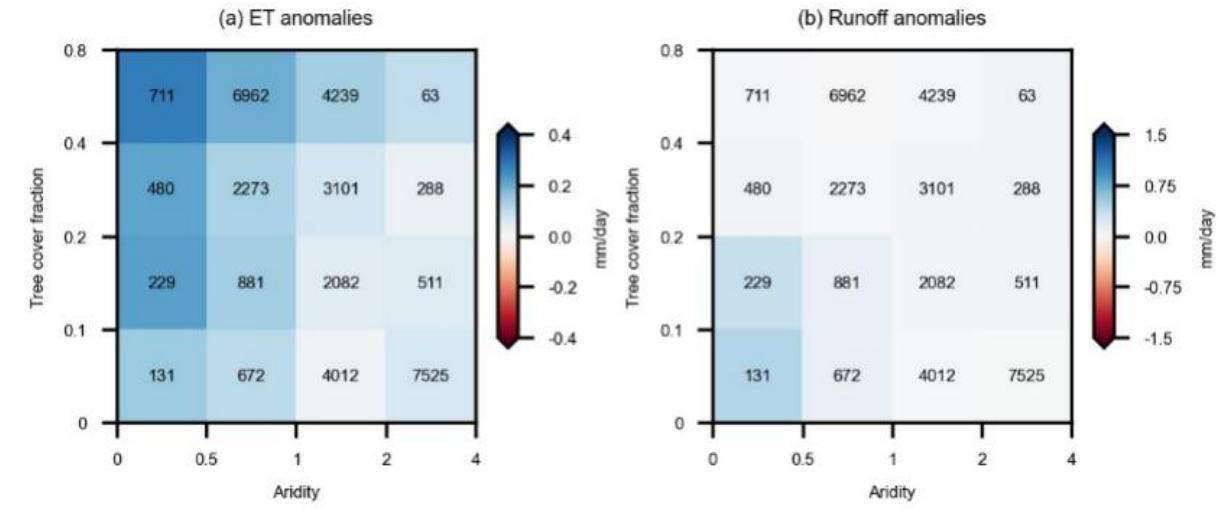

Figure S6: Same as Figure S5 but for ET and runoff anomalies at drought peaks expressed as the 75th percentile of value ranges across aridity and tree cover regimes.

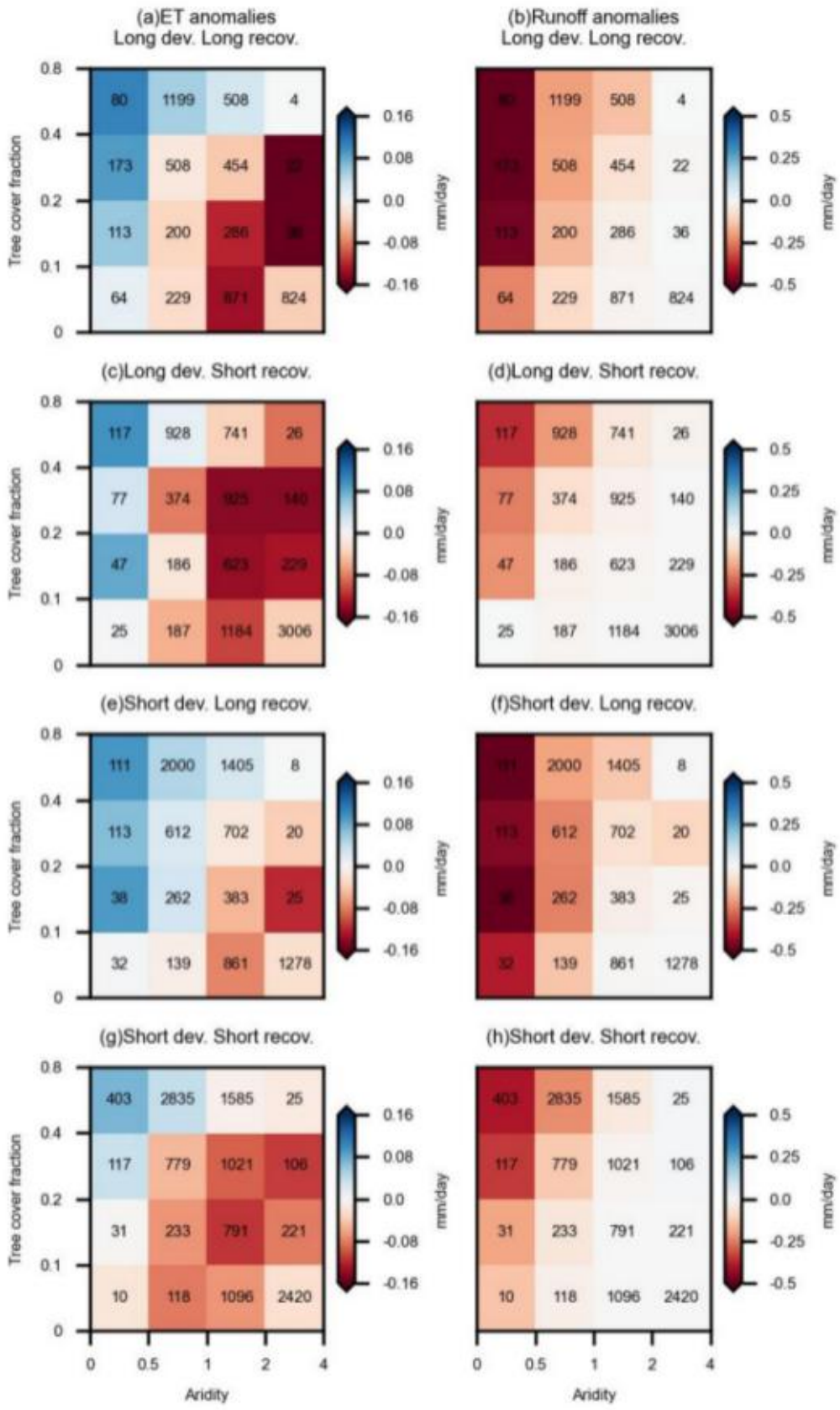
(a)ET anomalies
Long dev. Long recov.
(b)Runoff anomalies
Long dev. Long recov.
(c)Long dev. Short recov.
(d)Long dev. Short recov.
(e)Short dev. Long recov.
(f)Short dev. Long recov.
(g)Short dev. Short recov.
(h)Short dev. Short recov.
Tree cover fraction
Aridity
mm/day
0.8
0.4
0.2
0.1
0
0.5
1
2
4
0.16
0.08
0.0
-0.08
-0.16
0.25
-0.25
-0.5
80 1199 508 4
173 508 454 22
113 200 286 36
64 229 871 824
117 928 741 26
77 374 925 140
47 186 623 229
25 187 1184 3006
111 2000 1405 8
113 612 702 20
38 262 383 25
32 139 861 1278
403 2835 1585 25
117 779 1021 106
31 233 791 221
10 118 1096 2420

Figure S7: Similar as in Figure 3 but grouping grid cells with different drought duration. (a, b) The duration of drought development and recovery is above the 50th percentile of all existing duration values; (c, d) The duration of drought development is above the 50th percentile of all existing duration values, while the duration of drought recovery is below the 50th percentile; (e, f) The duration of drought recovery is above the 50th percentile of all existing duration values, while the duration of drought development is below the 50th percentile; (g, h) The duration of drought development and recovery is below the 50th percentile of all existing duration values.

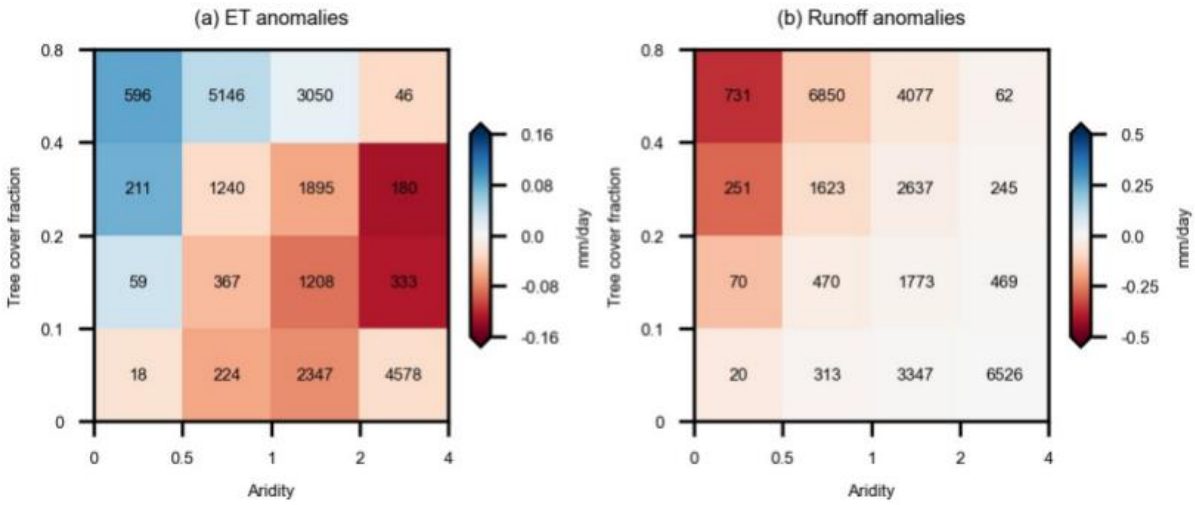

Figure S8: Similar as in Figure 3 but for the second drought selected by the second minimum soil moisture for each grid cell where it is at least 6-month before or after the first drought.

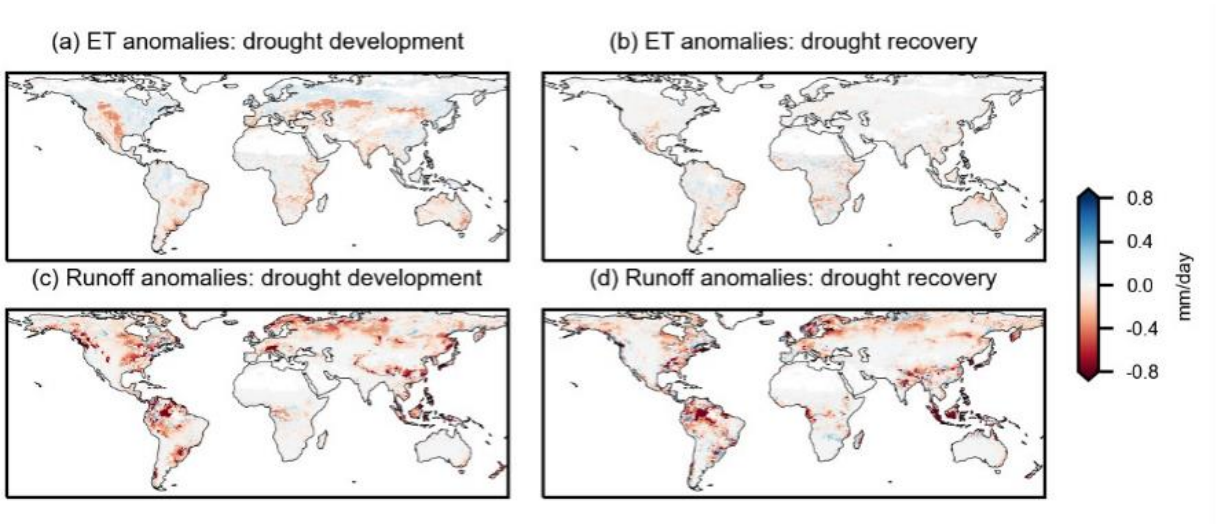

Figure S9: Observed global patterns of (a) ET anomalies during drought development, (b) ET anomalies during drought recovery, (c) runoff anomalies during drought development, and (d) runoff anomalies during drought recovery.

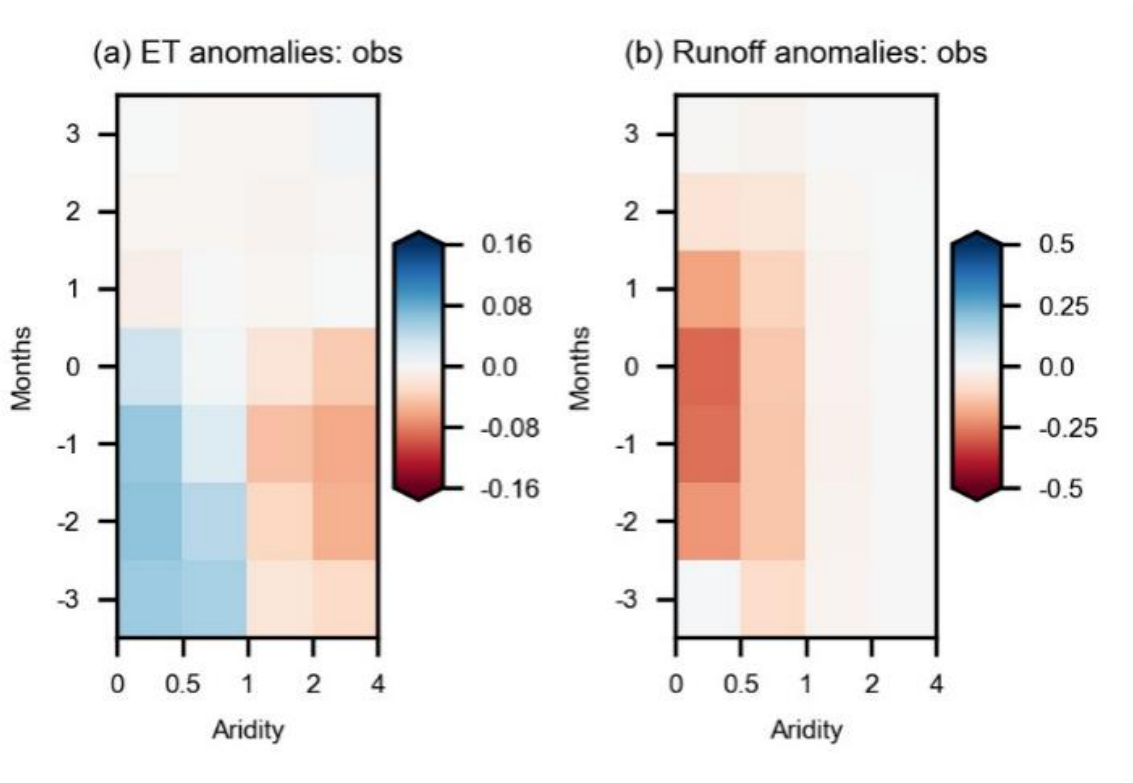

Figure S10: (a) ET and (b) runoff changes (mm/day) during the course of drought detected by GRACE total water storage grouped by aridity.

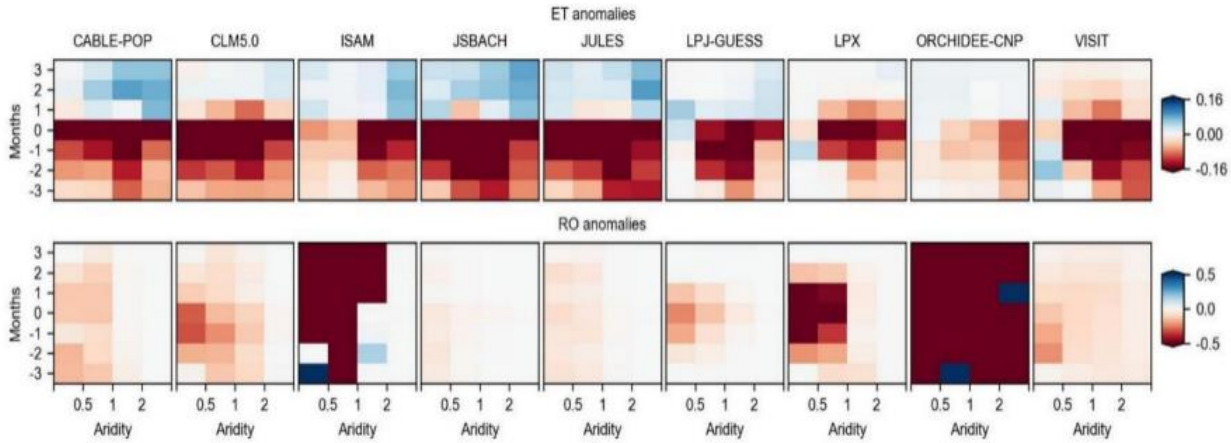

Figure S11: ET and runoff changes (mm/day) during the course of drought from individual LSMs grouped by aridity expressed as medians across grid cells. Month 0 denotes the drought peak months; negative months (-3, -2, -1) denote drought development periods and positive months (1, 2, 3) denote the drought recovery periods.

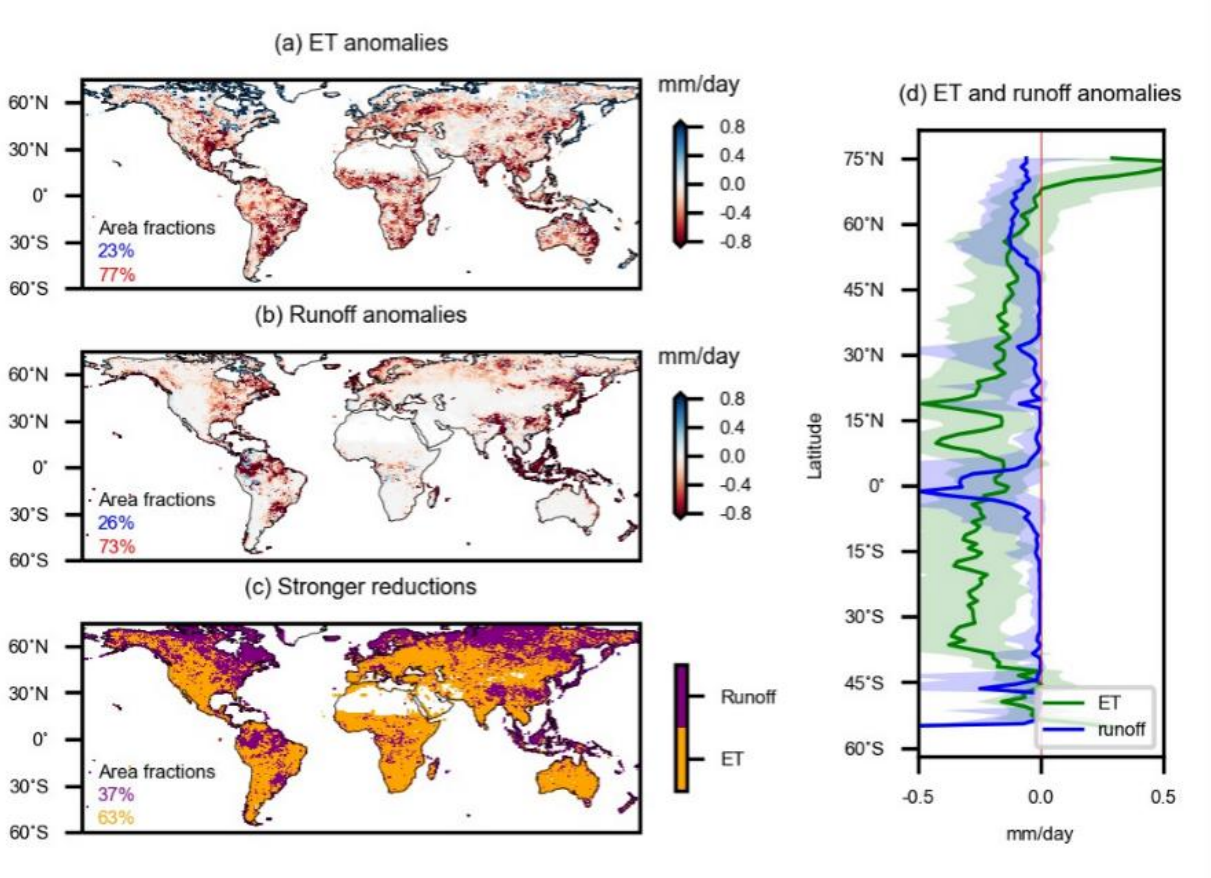

Figure S12: Similar as Figure 2 but for multi-model median values from LSMs. (a) ET and (b) runoff anomalies during the drought peak months. (c) Variable with stronger reductions. (d) Latitudinal patterns of displayed ET and runoff anomalies. The solid line and shaded areas show the median and interquartile ranges of ET and runoff anomalies across latitudes, respectively. In (a, b), area fractions are given for positive and negative changes, respectively, and in (c) area fractions are given where ET or runoff are more reduced during peak drought.

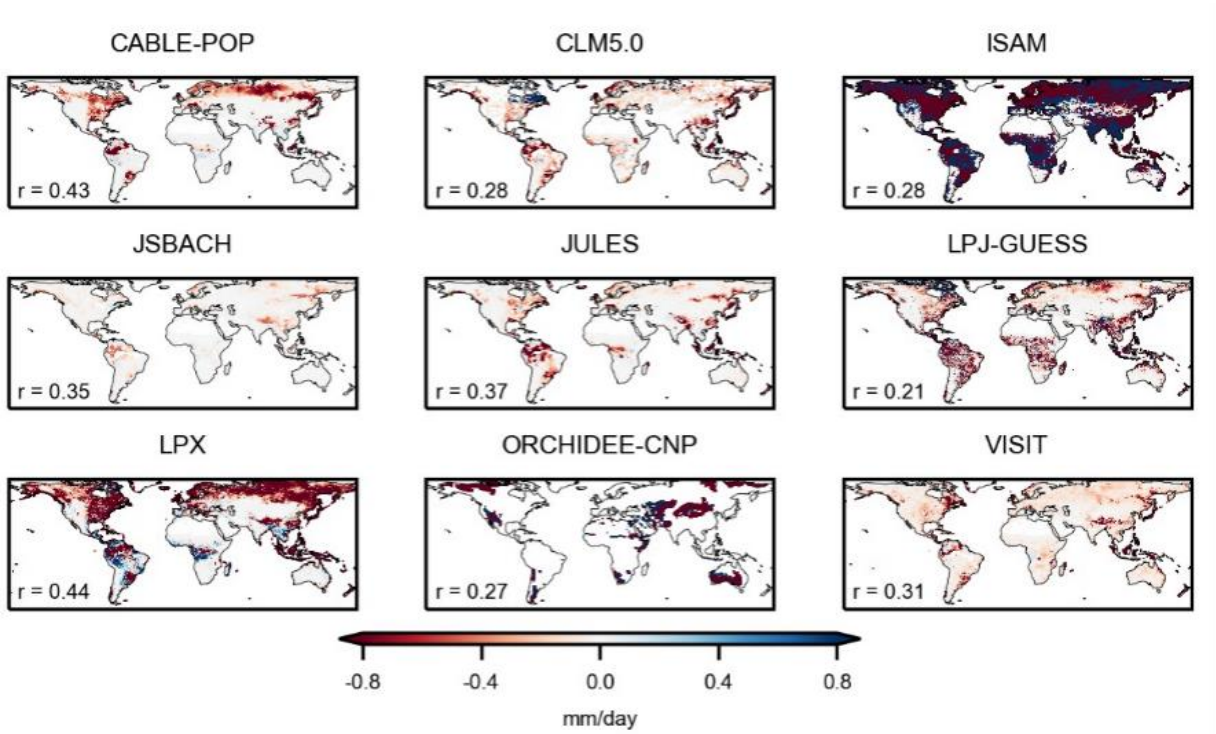

Figure S13: Spatial patterns of runoff anomalies during the drought peak month from individual LSMs. The r values denote spatial correlations with observation-based results in Figure 2b.

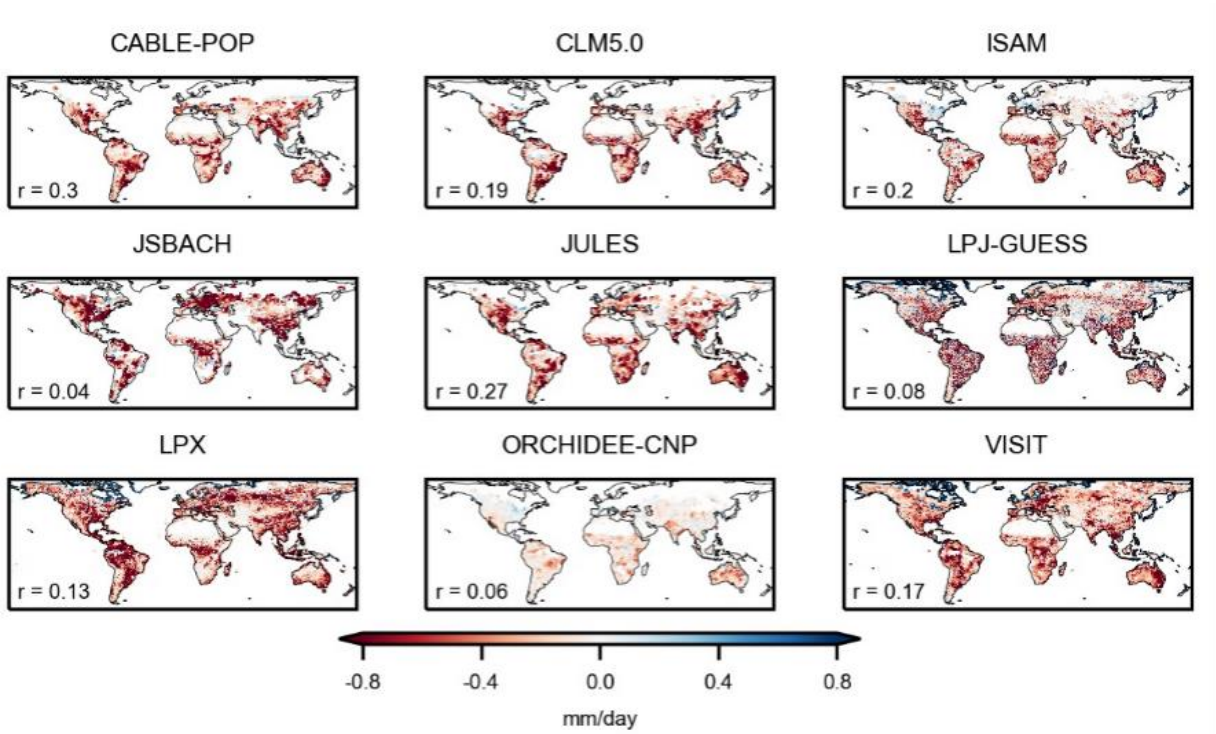

Figure S14: Spatial differences in ET anomalies during the drought peak months from individual LSMs. The r values denote spatial correlations with observation-based results in Figure 2a.

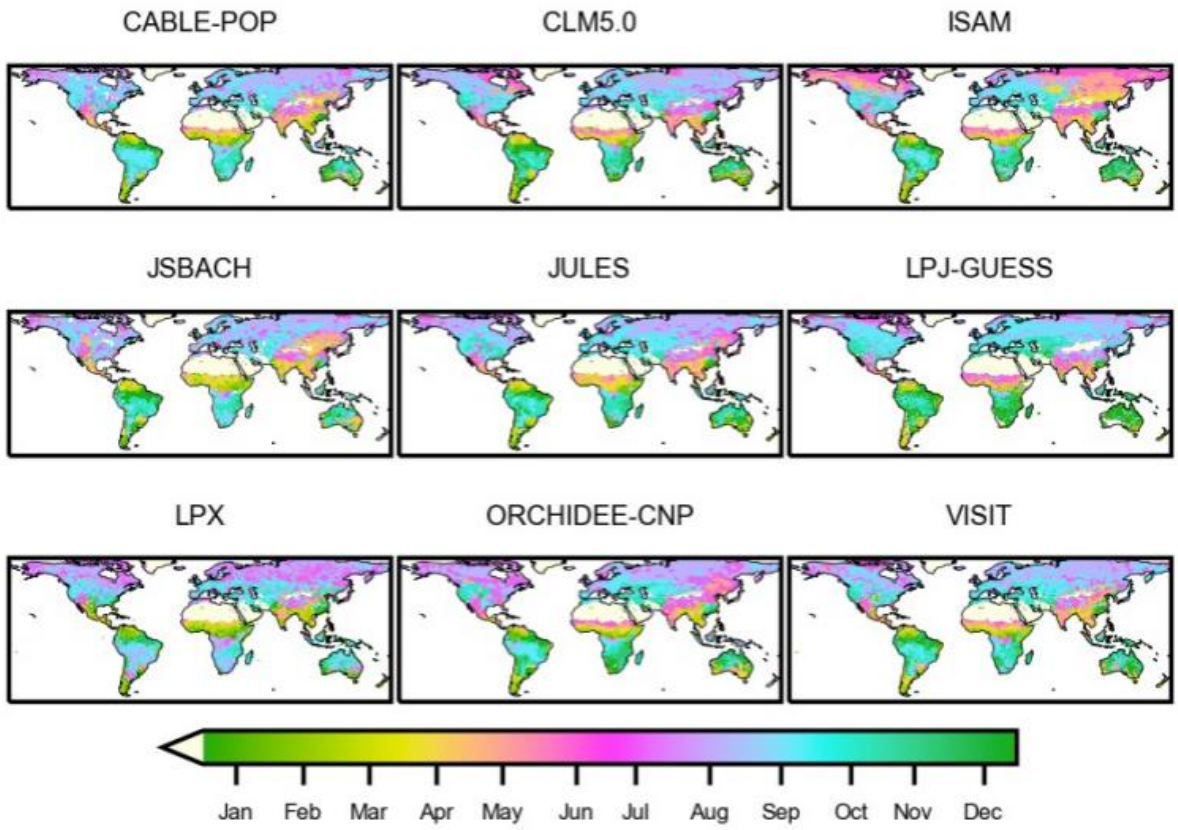

Figure S15: Months-of-year of drought peaks between 2001 to 2015 as detected from monthly total-column soil moisture simulated by LSMs.

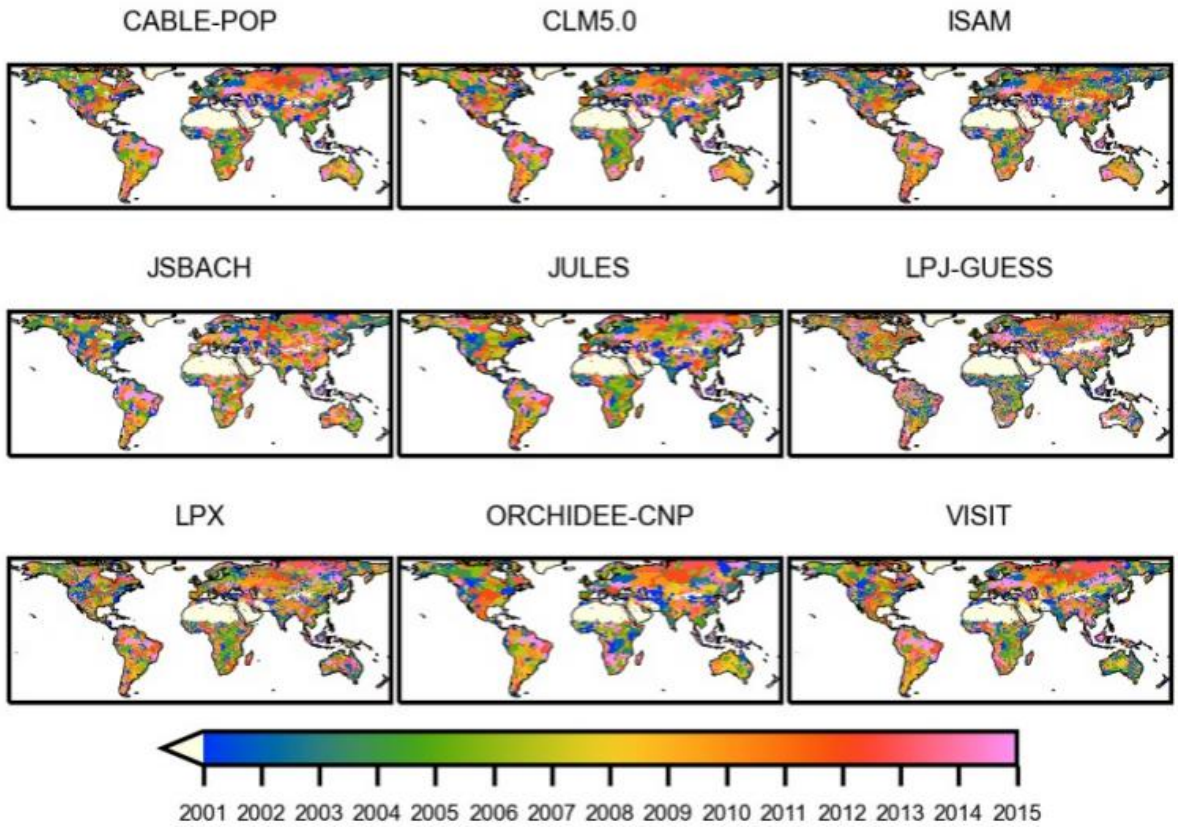

Figure S16: Years of drought peaks between 2001 to 2015 as detected from monthly total-column soil moisture simulated by LSMs.

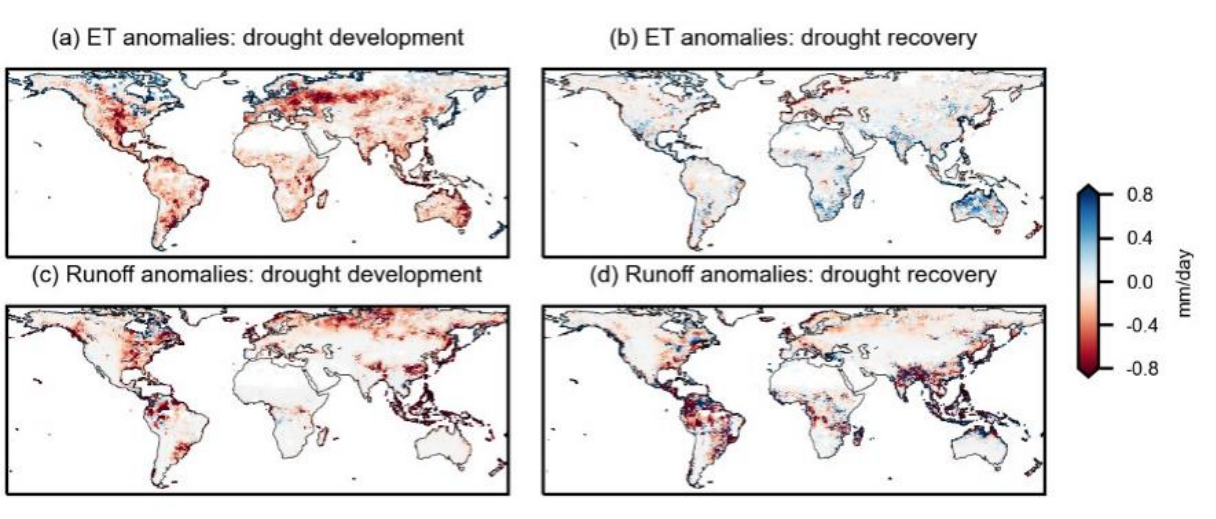

Figure S17: Global patterns of (a) ET anomalies during the drought development, (b) ET anomalies during the drought recovery, (c) runoff anomalies during the drought development, and (d) runoff anomalies during the drought recovery from median values of ensembles of land surface models.

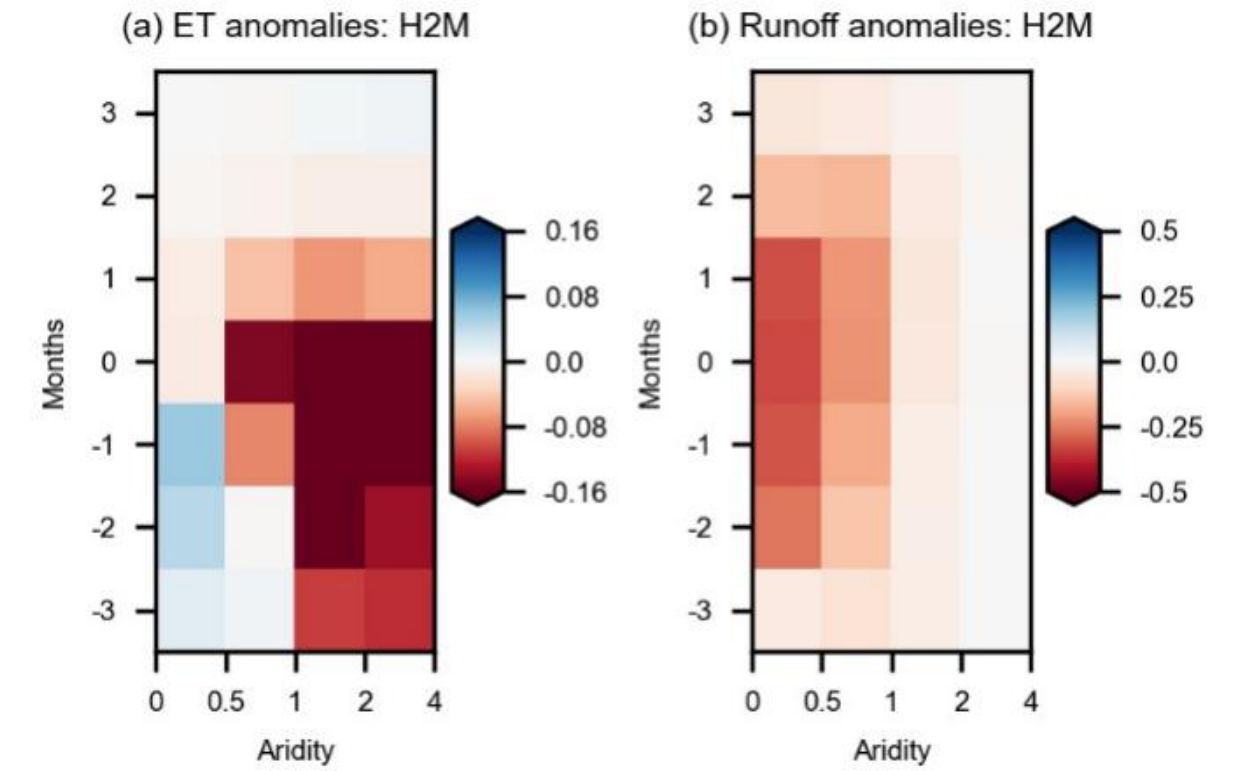

Figure S18: (a) ET and (b) runoff changes (mm/day) during the course of drought from H2M hybrid modeling outputs grouped by aridity.

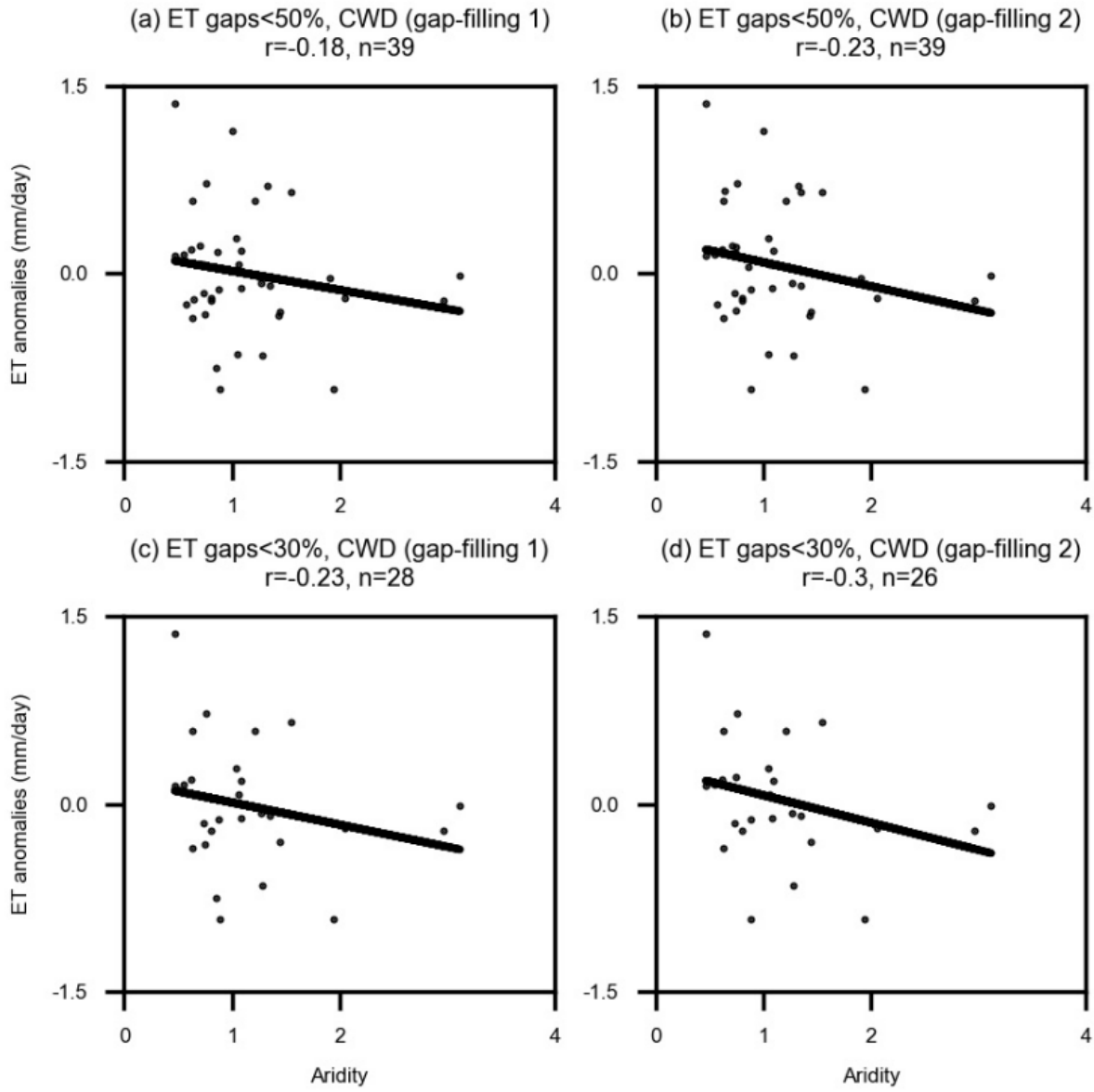

Figure S19: ET anomalies measured at flux towers during drought peak months are evaluated against aridity of each measurement site. The number of sites used for each panel is indicated with n. Hourly measurements are aggregated to monthly data; results are shown from sites with less than (a, b) 50% missing ET data and less than (c, d) 30% missing ET data, which are gap-filled using ET from GLEAM only for step of calculating cumulative water deficit (CWD). Drought peaks are detected through the monthly CWD where either gridded ERA5 precipitation is used to fill gaps (gap-filling 1) or downscaled ERAinterim precipitation is used to fill gaps using machine learning algorithms (gap-filling 2; Besnard et al., 2019).

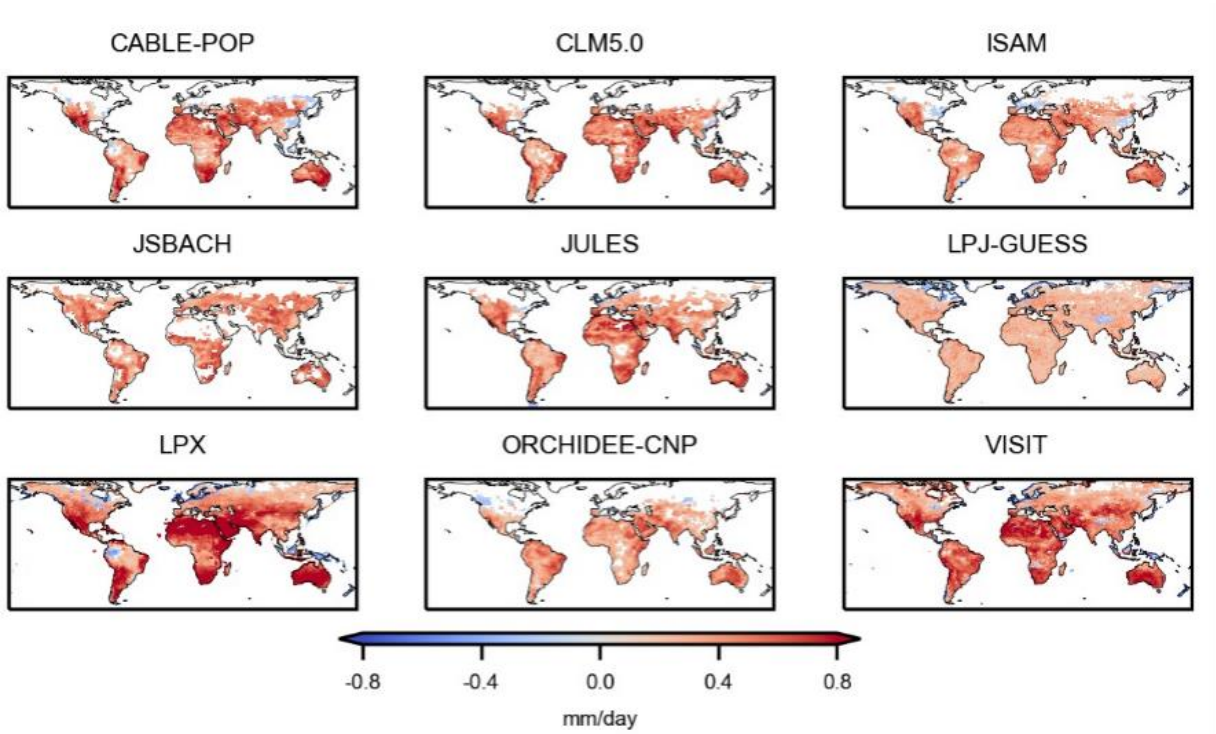

Figure S20: Monthly correlations between ET and soil moisture from individual models during 2001-2015. Two-sided significance tests are done for each colored grid cell at the $p<0.05$ level as assessed with Spearman correlation.

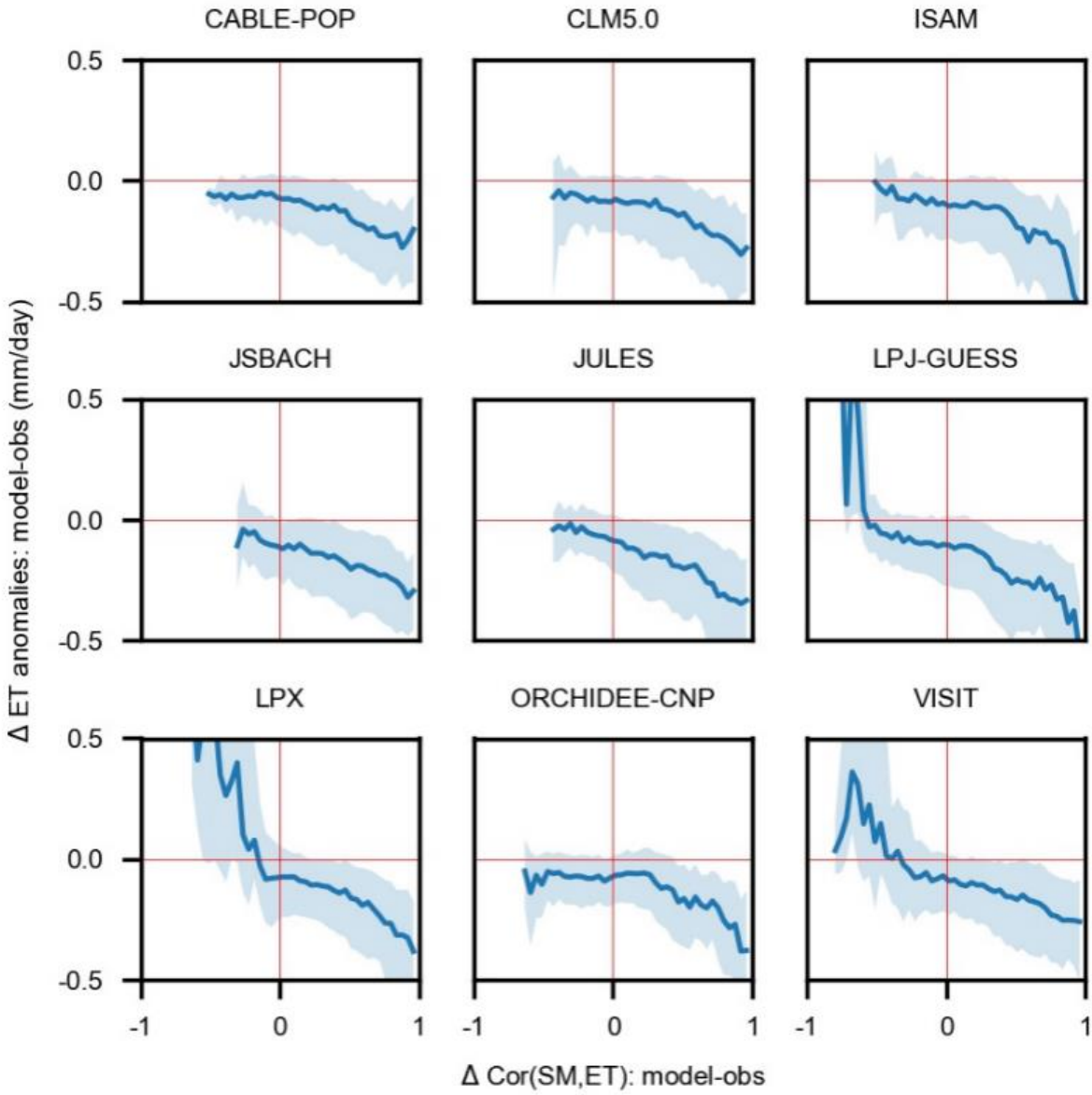

Figure S21: Relationships between biases of simulated ET anomalies at drought peaks (y-axis) and the respective differences between modeled and observed ET-soil moisture monthly relationships from 2001 to 2015 (x-axis). The solid lines denote median results and shaded areas denote interquartile ranges across spatial grid cells. Cor(SM, ET) denotes soil moisture-ET correlations. Two-sided significance tests are done for included grid cells at the $p<0.05$ level as assessed with Spearman correlation.

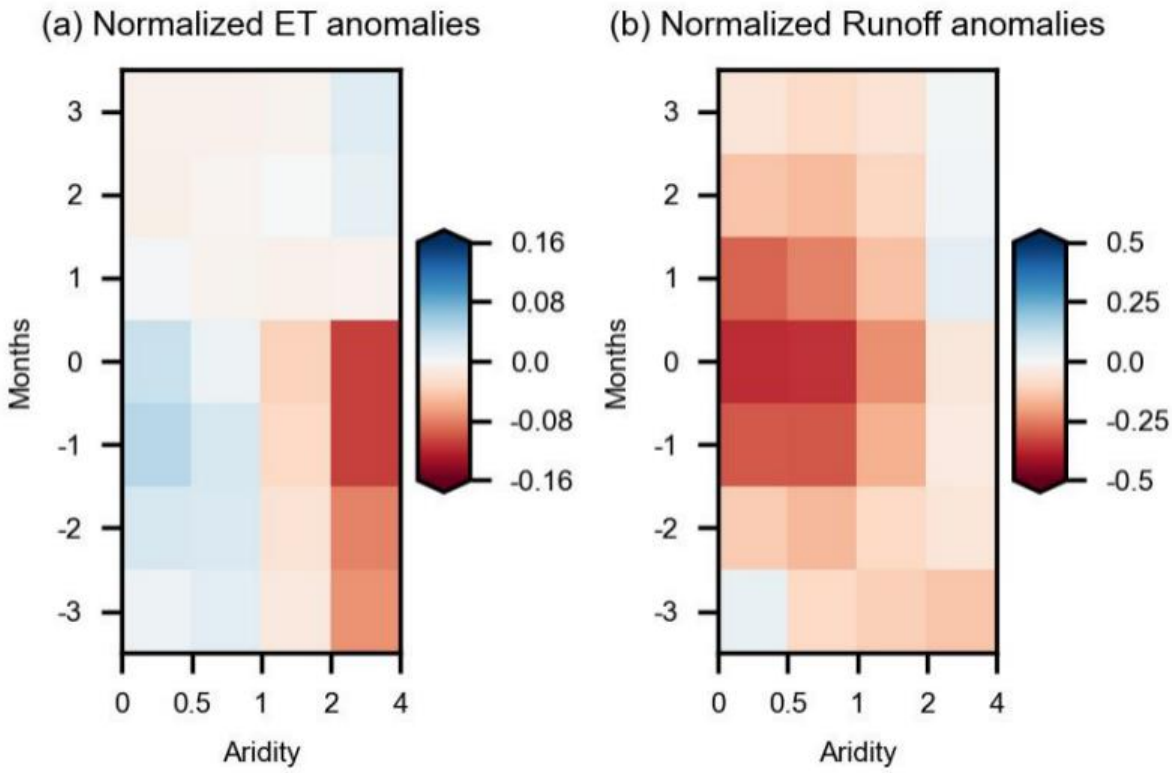

Figure S22: Similar to Figure 4 (a, b) but for ET and runoff anomalies divided by the respective mean seasonal values (unitless) during the course of drought.